V. MICROWAVE ELECTRONICS

Prof. L. D. Smullin   Prof. A. Bers   P. A. Mandics
Prof. H. A. Haus   Prof. L. J. Chu   H. M. Schneider

A. SUBMILLIMETER GENERATION WITH HIGH-DENSITY DRIFTING PLASMA

The generation of very high frequencies by means of a free electron stream is primarily limited by the electron densities that can be produced. In a semiconductor or semimetal plasma one can obtain electron densities several orders of magnitude larger than in free electron streams. Unlike the situation in free electron streams, however, in semiconductor plasmas the drift velocities, v_d, that can be imparted to the electrons are considerably limited and usually comparable with their thermal speed, v_T. Furthermore, the collision frequency, ν, is often greater than or at least comparable with the frequencies, ω, that we are interested in generating. At first thought, it may seem that under the condition $\nu > \omega$, in which the individual electrons are unable to serve as a memory for the signal, wave interactions would be highly damped. As we shall show in this report, this is not necessarily true. Thus, under the conditions $\omega_p \gg \nu$ and $\omega_p \gg \omega$, where ω_p is the plasma frequency, the collective behavior of the electrons predominates (and provides a memory), and lightly damped wave interactions are possible even when $\nu \gtrsim \omega$.

1. Free Waves

Consider a one-dimensional electron plasma uniformly drifting in the z direction with a velocity v_d. The drift velocity may be considered to be produced by an externally applied dc electric field E_0 in the z direction. We are interested in the longitudinal waves of such a system, and in this report shall use the simplest classical description of its dielectric constant within the framework of transport theory. Hence, in a reference frame in which the electrons have no drift, the dielectric constant is

$$K'(\omega', k') = 1 - \frac{\omega_p'^2}{-j\omega'(j\omega'+\nu') - k'^2 v_T'^2} \tag{1}$$

where ω' and k' are the frequency and longitudinal wave number associated with the time and space dependence $\exp j(\omega't'-k'z')$ of all field quantities, ω_p' is the plasma frequency, ν' is the collision frequency, and v_T' is the thermal velocity of the electrons. In the laboratory reference frame, in which the electrons have a drift velocity v_d, the dielectric constant for the slow longitudinal waves can be obtained by a nonrelativistic transformation

$$\omega' = \omega - kv_d \tag{2}$$

$$k' = k \tag{3}$$

with $\omega_p' = \omega_p$, $\nu' = \nu$, and $v_T' = v_T$. The result is

$$K(\omega, k) = 1 - \frac{\omega_p^2}{(\omega - kv_d)^2 - j\nu(\omega - kv_d) - k^2 v_T^2}, \tag{4}$$

where the time and space dependence of all field quantities is $\exp j(\omega t - kz)$.

The dispersion relation is obtained from

$$K(\omega, k) = 0. \tag{5}$$

It can be checked that there are no possible instabilities in this system. Thus Eqs. 4 and 5 give

$$\omega = kv_d + j\frac{\nu}{2} \pm \sqrt{\omega_p^2 + k^2 v_T^2 - \frac{\nu^2}{4}}, \tag{6}$$

which for real k has solutions with the imaginary part of ω only positive, therefore signifying decay in time. But for real k with

$$\omega_p^2 + k^2 v_T^2 > \frac{\nu^2}{4} \tag{7}$$

and

$$kv_d \gg \frac{\nu}{2}, \tag{8}$$

the decay rate per period of oscillation may be made very small, and lightly damped waves should be possible.

Next we look at the steady-state solutions of the dispersion relation, Eqs. 4 and 5 for real ω, and find

$$kv_d = \frac{\left(\omega - j\frac{\nu}{2}\right) \pm \sqrt{\left(\omega - j\frac{\nu}{2}\right)^2 + \left(\omega_p^2 - \omega^2 + j\nu\omega\right)\left(1 - \frac{v_T^2}{v_d^2}\right)}}{\left(1 - \frac{v_T^2}{v_d^2}\right)}. \tag{9}$$

Hence, if $\nu > \omega$, waves with a spatial decay rate that is small compared with a wavelength can be obtained if

$$v_d > v_T \tag{10}$$

$$\omega_p^2 \gg \frac{\omega^2}{1 - \frac{v_T^2}{v_d^2}} \tag{11}$$

and

$$\omega_p^2 \gg \frac{\nu^2}{1 - \frac{v_T^2}{v_d^2}}.$$ (12)

Under these conditions, we have approximately

$$k \approx \pm \frac{\frac{\omega_p}{v_d}}{\left(1 - \frac{v_T^2}{v_d^2}\right)^{1/2}},$$ (13)

and the positive solution can be shown to correspond with a negative small-signal energy wave. Interaction of a proper circuit with this wave should result in the extraction of energy from this system and thus produce oscillators and amplifiers. In semiconductors and semimetals the conditions in Eqs. 11 and 12 can be satisfied even in the submillimeter regime; Eq. 11 is necessary, since $\nu \sim \omega$. The condition of Eq. 10 will require high dc fields, and possibly cooling of the material.

2. Interaction in a One-Dimensional Gap

The simplest circuit interaction that we have studied is the one-dimensional gap shown in Fig. V-1a. The equation for the currents is

$$j\omega \epsilon E + J = K,$$ (14)

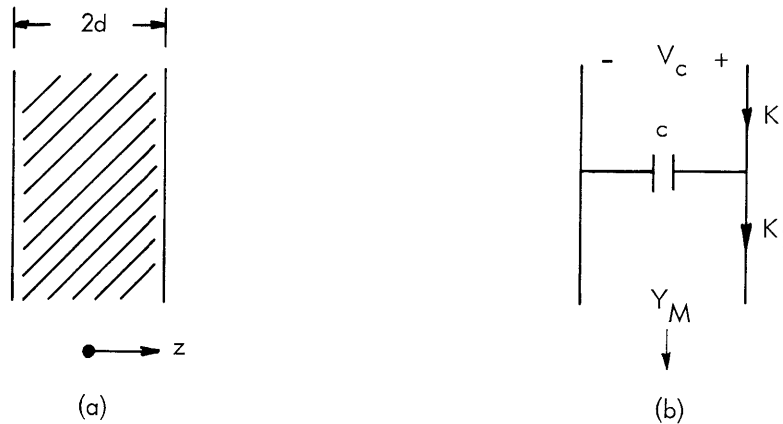where E is the longitudinal electric field, J is the longitudinal electron current density,

Fig. V-1. (a) One-dimensional plasma gap. (b) Equivalent circuit.

and K is the current density in the external circuit. The circuit equation is obtained by integrating Eq. 14 over the gap length. We have

$$j\omega c \, V_c + K_i = K, \tag{15}$$

where

$$c = \frac{\epsilon}{2d} \tag{16}$$

$$V_c = \int_{-d}^{d} E \, dz \tag{17}$$

$$K_i = \frac{1}{2d} \int_{-d}^{d} J \, dz \tag{18}$$

The equivalent circuit is shown in Fig. V-1b. K_i is the current induced as a result of the interaction with the medium. The excitation of the medium by the circuit follows from the equations of motion and continuity, and Eq. 14.

$$\left[\left(v_d^2 - v_T^2 \right) \frac{\partial^2}{\partial z^2} - 2\left(\omega - j\frac{\nu}{2} \right) v_d \frac{\partial}{\partial z} - \left(\omega_p^2 - \omega^2 + j\nu\omega \right) \right] J = \omega_p^2 K. \tag{19}$$

The interaction is described completely by the simultaneous solution of Eqs. 14-19. The quantity of primary interest is the loading of the circuit by the medium, as shown in Fig. V-1b. Thus

$$Y_M = \frac{K_i}{V_c}. \tag{20}$$

From Eqs. 13-19 we find

$$Y_M = \frac{Y}{1 - \dfrac{Y}{j\omega c}} \equiv G_M + jB_M, \tag{21}$$

where

$$Y = y_1 \frac{\left(1 - M_1 \, e^{-jk_1 d} \right)}{jk_1 2d} + y_2 \frac{\left(1 - M_2 \, e^{-jk_2 d} \right)}{jk_2 2d} \tag{22}$$

$$M_{1,2} = \frac{e^{jk_{1,2}d} - e^{-jk_{1,2}d}}{jk_{1,2}2d} \tag{23}$$

$$y_{1,2} = \frac{Y_{1,2} Y_{2,1}}{Y_{2,1} - Y_{1,2}} \tag{24}$$

$$Y_{1,2} = -\frac{\omega\epsilon\,\dfrac{\omega_p^2}{v_d^2}}{k_{1,2} - \dfrac{\omega}{v_d}} \tag{25}$$

and $k_{1,2}$ is given by Eq. 9. For a given set of parameters describing the plasma $(\omega_p, \nu, v_d, v_T)$ Eq. 21 can be evaluated at the frequencies, ω, of interest and for various
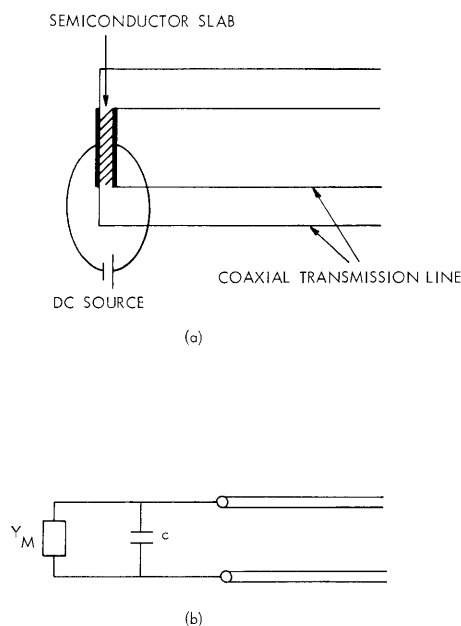

Fig. V-2. (a) Possible circuit configuration of a one-gap device. (b) Equivalent circuit. With Re $Y_M < 0$, the device can be used as an oscillator or amplifier.

gap lengths, 2d. Whenever $G_M < 0$ we have the possibility of an oscillator (or with an external circulator, an amplifier device) as shown schematically in Fig. V-2.

3. Evaluation of the Medium Admittance Y_M

In this report we shall show some calculations of Y_M for the case $\nu = 0$ and $v_T = 0$. This case is purely of theoretical interest and is simply an extension of previously reported calculations for high-density electron streams.[1] In the future parameters will be so chosen as to apply to some common semiconductors at very low temperatures.

a. High-Density Electron Stream Gap: $\nu = 0$, $v_T = 0$

The calculations are illustrated in Figs. V-3 and V-4. Here, $Y_M \equiv Y_{e\ell}$, as in our previous report,[1] and the values of ω_p/ω were chosen higher than before.[1] We note that
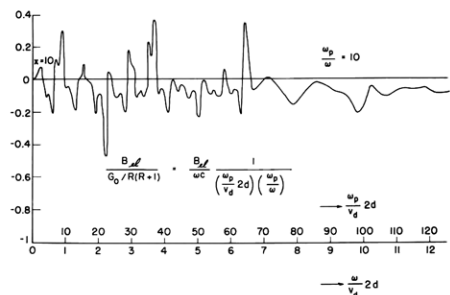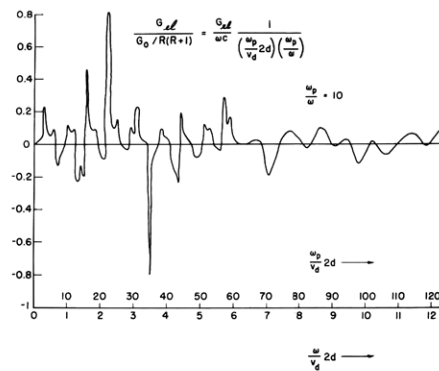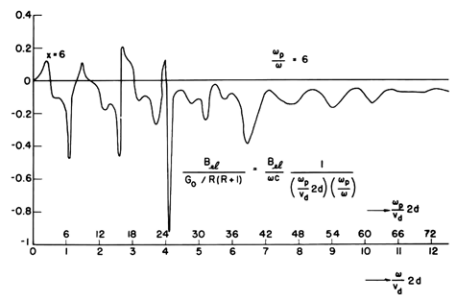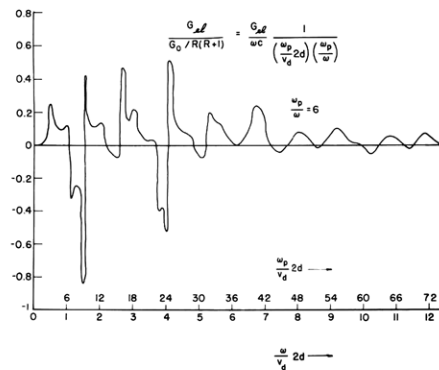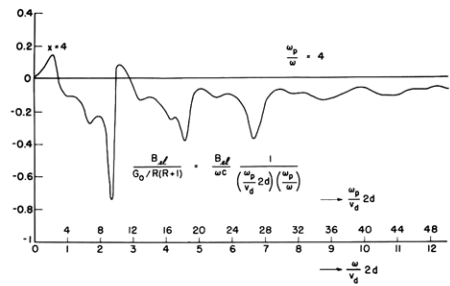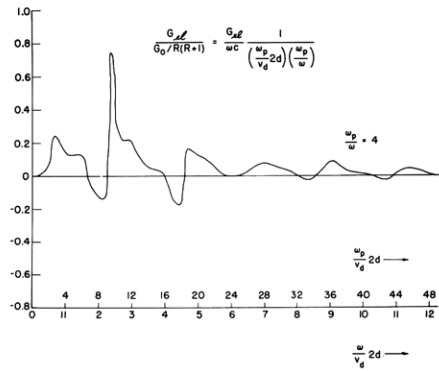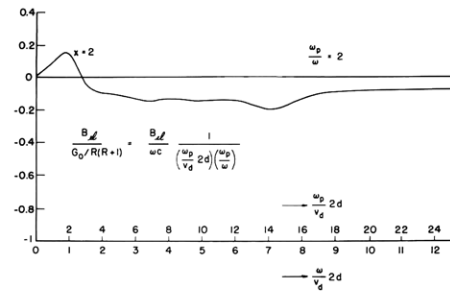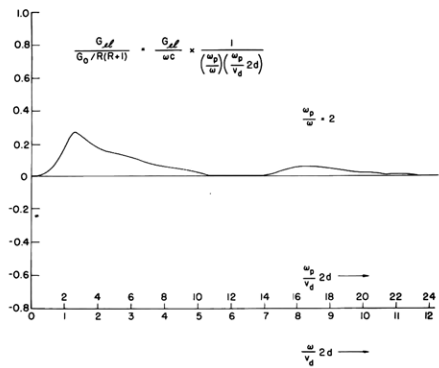
Fig. V-3. Real part of medium loading admittance for free electron stream ($\nu = 0$, $v_T = 0$). $\left[Y_M = Y_{e\ell}\right.$ of previous report.[1]$\left.\right]$

Fig. V-4. Imaginary part of medium loading admittance for free electron stream ($\nu = 0$, $v_T = 0$). $\left[Y_M = Y_{e\ell}\right.$ of previous report.[1]$\left.\right]$

there are several regions of appreciably negative $G_{e\ell}$.

Computations for larger ranges of (ω_p/v_d) 2d, and on the effect of finite temperatures and collisions are being carried out.

A. Bers

References

1. A. Bers, Exact solution of the small-signal, one-dimensional, gap interaction for neutralized, relativistic, electron streams, Quarterly Progress Report No. 63, Research Laboratory of Electronics, M. I. T., October 15, 1961, pp. 89-101.

B. HIGH-PERVEANCE HOLLOW ELECTRON-BEAM STUDY

Measurements have been completed on the DC and RF interaction performance of an electron beam produced by a conical-cathode, magnetron injection gun. A detailed description of the system and some of the measurements have been given in a previous report.[1]

1. D-C Performance of the Gun

The DC characteristics of the conical-cathode gun reported previously[1] have been
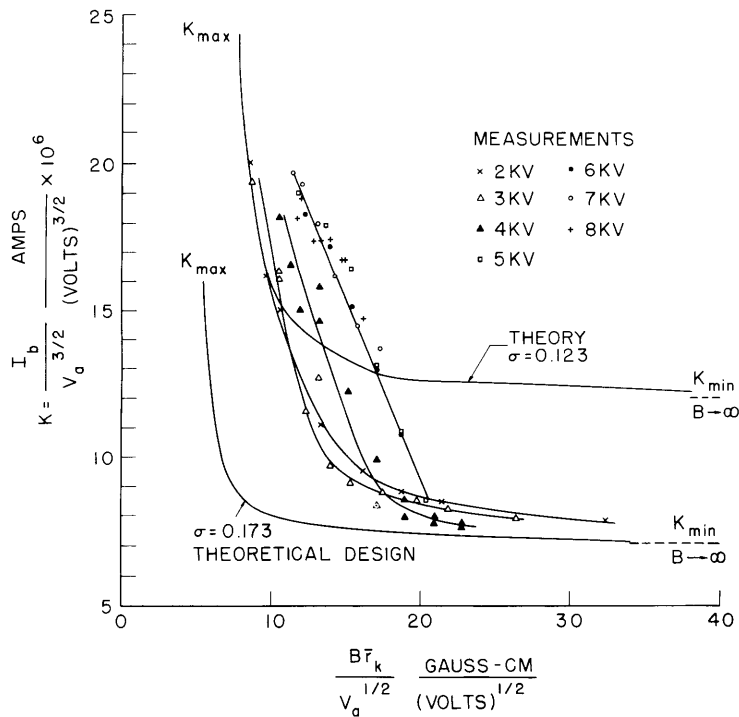

Fig. V-5. D-C performance characteristics of conical-cathode magnetron injection gun.

compared with the simple design theory based on a planar cathode.[2,3] The results are shown in Fig. V-5. The theoretical curves were derived by using a technique developed by Arnaud, Wendt and Gueuard.[4] The maximum perveance $I_b/V_a^{3/2}$ (obtained when the beam grazes the front of the anode) is given by

$$K_{max} = \frac{\pi \epsilon_o \sqrt{2\eta}}{9} \frac{\bar{r}_k}{\ell_k} \frac{\sin^2 \theta \cos^2 \theta}{\left[\sin \theta \cos \theta \left(\frac{\sigma}{6} + \frac{\tan \theta}{12} \right) \right]^{3/2}}. \tag{1}$$

Here, $\eta = |e|/m$, $\bar{r}_k$ is the average cathode radius, ℓ_k is the length of the cathode, θ is the cathode cone half-angle, and

$$\sigma = \frac{s}{\ell_k}. \tag{2}$$

Here, s is the distance between the anode and the cathode at the front end of the cathode. At this maximum perveance we also have

$$\left(\frac{B\bar{r}_k}{V_a^{1/2}} \right)_{K_{max}} = \frac{\sqrt{\frac{2}{\eta}} \frac{\bar{r}_k}{\ell_k}}{(\sigma - \tan \theta) \left[\frac{2\left(\sigma - \frac{1}{4}\tan \theta \right)}{(\sigma - \tan \theta)} - 1 \right]^{1/2}}. \tag{3}$$

The minimum perveance (obtained when $B \to \infty$) is given by

$$K_{min} = \frac{\pi \epsilon_o \sqrt{2\eta}}{9} \frac{\bar{r}_k}{\ell_k} \frac{\sin^2 \theta \cos^2 \theta}{\left[\sin \theta \cos \theta \left(\frac{\sigma}{3} - \frac{\tan \theta}{12} \right) \right]^{3/2}}. \tag{4}$$

It is clear from Fig. V-5 that the minimum perveance agrees well with the theoretical
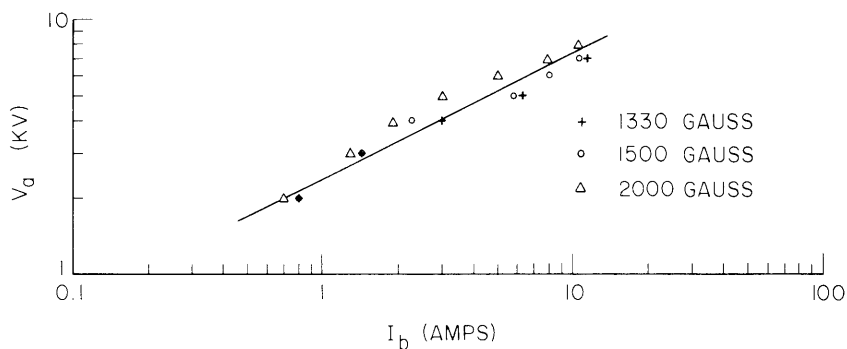

Fig. V-6. Voltage vs current for constant magnetic field in the conical-cathode gun.

Table V-1. Conical-cathode gun DC characteristics (drift-tube radius a = 0.952 cm).

Case	V_a (kv)	V_b (kv)	I_b (amp)	B_o (gauss)	K (microperv)	$\dfrac{b-c}{b}$	$\dfrac{a}{b}$	f_p (mc)
1	2.4	2.23	1.7	1000	14.5	0.193	1.18	650
2	2.4	2.25	1.3	1330	10.6	0.138	1.22	675
3	3.0	2.74	3.3	1000	20.0	0.234	1.18	799
4	3.0	2.80	2.0	1330	12.1	0.163	1.19	729
5	3.5	3.17	4.4	1000	21.2	0.286	1.14	785
6	3.5	3.28	2.5	1500	12.1	0.173	1.19	760
7	4.0	3.66	3.9	1500	15.4	0.167	1.20	945

Table V-2. Conical-cathode gun electronic beam loading (cavity-gap length 2d = 0.444 cm; f_o = 1120 mc).

Case	$G_{e\ell}$ Measurement $((ohm)^{-1} \times 10^6)$	Calculation — Kinematic Theory Thin Beam (b≈c) $((ohm)^{-1} \times 10^6)$	Calculation — Space-Charge Theory Thin Beam (b≈c) $((ohm)^{-1} \times 10^6)$
1	142	107	110
2	93.6	79.8	76.7
3	233	174	174
4	127	102	105
5	319	200	200
6	168	109	107
7	252	147	150

Table V-3. Conical-cathode gun space-charge wavelength and two-cavity klystron gain (cavity-gap length 2d = 0.444 cm; f_o = 1120 mc).

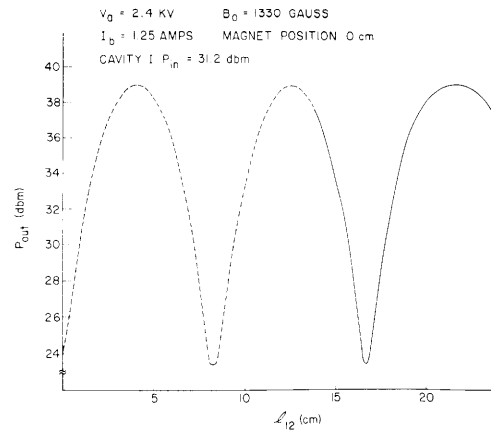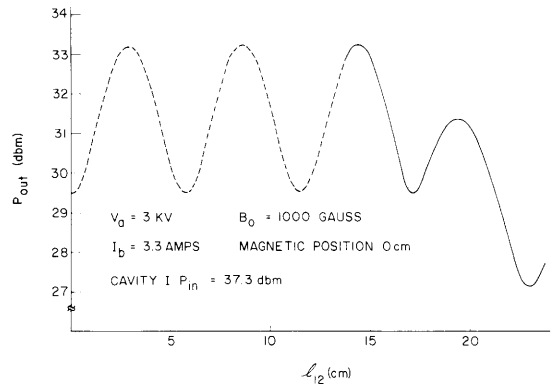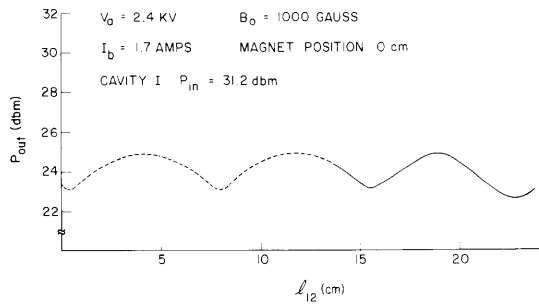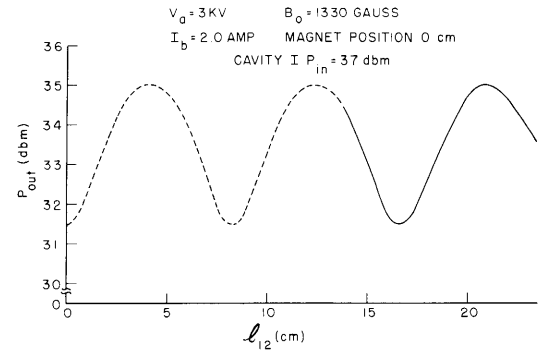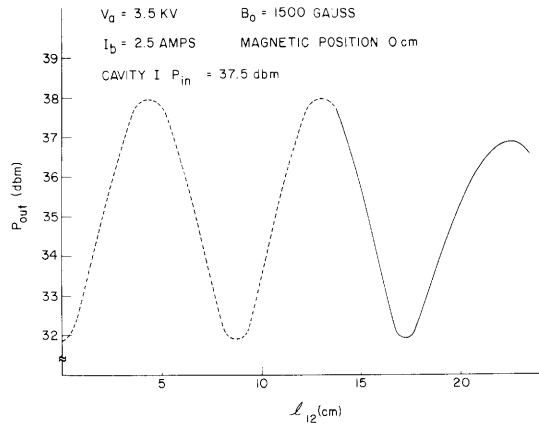| Case	Measurement λ_q (cm)	Measurement Gain (db)	Calculation λ_q (cm)	Calculation Gain (db)	M^2	$Y_o M^2$ $((ohm)^{-1} \times 10^3)$
1	14.8	-6.3	14.5	7.34	0.397	0.894
2	16.8	7.8	16.1	9.44	0.392	0.731
3	11.5	-4.1	12.1	2.67	0.445	1.11
4	16.6	-2.0	16.7	7.5	0.465	0.986
5	—	—	12.8	1.34	0.488	1.46
6	17.3	0.45	17.8	5.82	0.500	1.09
7	—	—	16.1	4.98	0.535	1.42

Fig. V-7. Second-cavity power output vs distance between cavity gaps. Electron beam from conical-cathode gun. Uniform magnetic field.

design. For low magnetic fields, because of the fact that the theoretical design has neglected the centrifugal force, the observed perveance is much higher, and the gun behavior is that of one whose anode is closer to the cathode (σ approximately 30 per cent smaller).

In Fig. V-6 the experimental data have been plotted for constant magnetic-field values. We note that to a good approximation the characteristic is $I_b \sim V_a^2$, as might be expected in a crossed-field gun.

b. RF Performance of the Beam

The rf interaction measurements with cavities along the beam were continued with a high-power AML 011-29 stable pulsed-signal source (courtesy of Spencer Laboratory, Raytheon Manufacturing Company). A beam pulse of 4 μsec and a synchonized 1-μsec rf pulse were used. The measured and calculated dc parameters are given in Table V-1. The results of the beam-loading measurements are presented in Table V-2. In order to compare the real part of the electronic admittance, $G_{e\ell}$, with theory, $G_{e\ell}$ was calculated by using the kinematic[5] and space-charge[6] theories and assuming a thin beam (b-c $\ll$c). The substantially increased rf power input made it possible to take considerably more accurate electronic loading measurements than we had done previously.[1]

The results of the space-charge wavelength and two-cavity gain measurements are plotted in Fig. V-7. The theoretical space-charge wavelength and gain values were calculated in the same way as before.[1] These theoretical and experimental results are compared in Table V-3. In spite of the increased rf power input into the system, the measured and calculated gain values still show a marked discrepancy in most cases. The measured values of electronic loading and space-charge wavelengths for thin beams
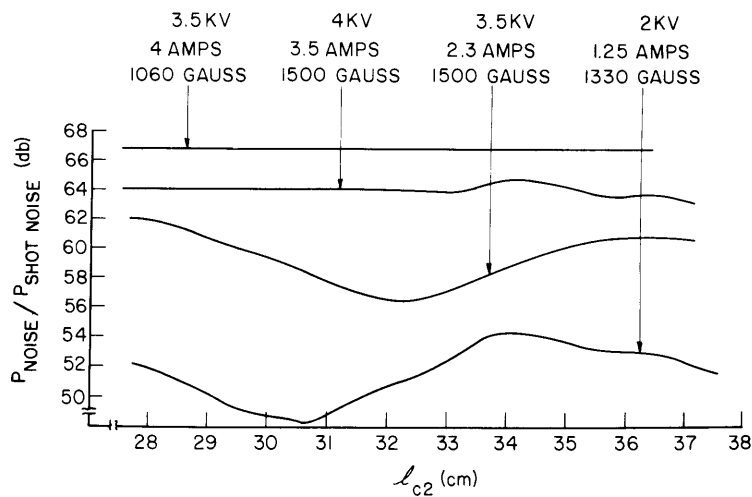

Fig. V-8. Second-cavity noise power output vs distance between cathode and cavity gap. Electron beam from conical-cathode gun. Uniform magnetic field.

(15 per cent) are in good agreement with the calculated values.

The noise-power output from the second cavity is shown in Fig. V-8 for four different voltage settings. As we have noted in our previous report, unlike that along a beam from a cylindrical cathode, the noise along the beam from a conical cathodes does not exhibit growth. In fact, for low voltages and high magnetic fields the noise along the beam exhibits a standing-wave pattern of the fundamental space-charge wavelength. As can be seen from Fig. V-8, in all cases the average noise level is extremely high and increases with increasing beam voltage.

A. Bers, P. Mandics

References

1. P. A. Mandics and A. Bers, Quarterly Progress Report No. 70, Research Laboratory of Electronics, M.I.T., July 15, 1963, pp. 43-57.

2. A. Bers, L. Anderson, and K. Keller, Theory and Design of a Conical Electron Gun for Producing a Hollow Beam, Spencer Laboratory-Engineering Report No. PT-277, Raytheon Company, Burlington Mass., 1962.

3. G. S. Kino and N. S. Taylor, The design and performance of a magnetron injection gun, IRE Trans., Vol. ED-9, p. 1, January 1962.

4. J. Arnaud, G. Wendt, and P. Gueuard, Research on the Instability in the Hollow Beam, Report WR 1005, CSF-France, March 1963 (unpublished).

5. A. Bers, Kinematic theory of gap interaction for relativistic electron beams, Quarterly Progress Report No. 66, Research Laboratory of Electronics, M.I.T., July 15, 1962, pp. 29-30.

6. A. Bers, Linear Space-Charge Theory of Gap Interaction between an Electron Beam and Electromagnetic Fields, NTF 221, 53-60 (1961).

C. COMPLEX WAVES IN ELECTRON-BEAM WAVEGUIDES

The existence of complex propagation constants $(\gamma = \alpha + j\beta; \exp -\gamma z)$ in electron-beam waveguides has been known since the early days of the development of space-charge wave theories.[1,2] In comparison with the study of the purely propagating space-charge waves, little attention has been given to complex waves. In this report we review the existence of the complex waves and their properties and show their importance in providing a possible feedback mechanism in electron-beam devices.

1. Natural Waves

In order to illustrate the occurrence of complex waves, consider the simple example of a cylindrical waveguide filled with a uniform electron beam that is confined by an infinite magnetic field along the waveguide axis, z. The linearized equation of motion and Maxwell's equations, with all field quantities having the dependence $\exp(j\omega t - \gamma z)$, lead to the dispersion relation[1,2]

$$p^2 = (\gamma^2 + k^2) \left[1 + \frac{\beta_p^2}{(j\beta_e - \gamma)^2} \right]$$ (1)

where $k = \omega/c$, $\beta_e = \omega/v_o$, and $\beta_p = \omega_p/v_o$, with v_o the unperturbed electron velocity and ω_p the plasma frequency in the laboratory reference frame. The transverse wave

ELECTRON BEAM
PERFECTLY CONDUCTING DRIFT TUBE (WAVEGUIDE)
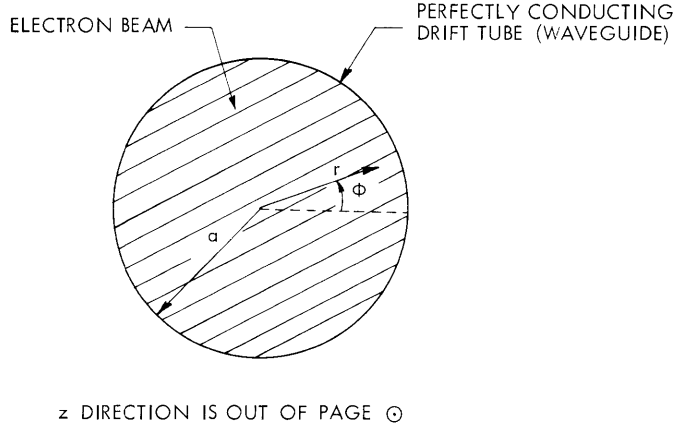
z DIRECTION IS OUT OF PAGE ⊙

Fig. V-9. Circular, filled, electron-beam waveguide.

number p is determined by the boundary conditions on the z component of the electric field at the perfectly conducting wall of the waveguide. For a waveguide of circular cross section (see Fig. V-9) and for modes with no azimuthal variation we have

$$J_o(pa) = 0,$$ (2)

where $J_o(x)$ is the zero-order Bessel function of the first kind, and a is the waveguide radius.

Equation 1 is a fourth-order algebraic equation for the propagation constant γ for each solution of Eq. 2. In this report, the allowable propagation constants γ will be discussed for a particular solution p to Eq. 2.

For $\beta_p < p$, a plot of the propagation constant γ against ω is shown in Fig. V-10. For frequencies below the empty-waveguide cutoff frequency, pc, there are two pure imaginary values of γ of the form $\gamma = j\beta$, as well as two complex values of γ, $\gamma = \alpha + j\beta$ and $(-\gamma^*) = -\alpha + j\beta$. The pure imaginary roots are the well-known space-charge waves.[1-3] The complex roots exist in the pairs γ and $(-\gamma^*)$, and hence have equal imaginary parts but oppositely signed real parts. The complex waves decay in space with an attenuation constant α.

For frequencies above the empty-waveguide cutoff frequency, pc, there are four pure imaginary values of γ: the two space-charge waves and the fast waves.[4]
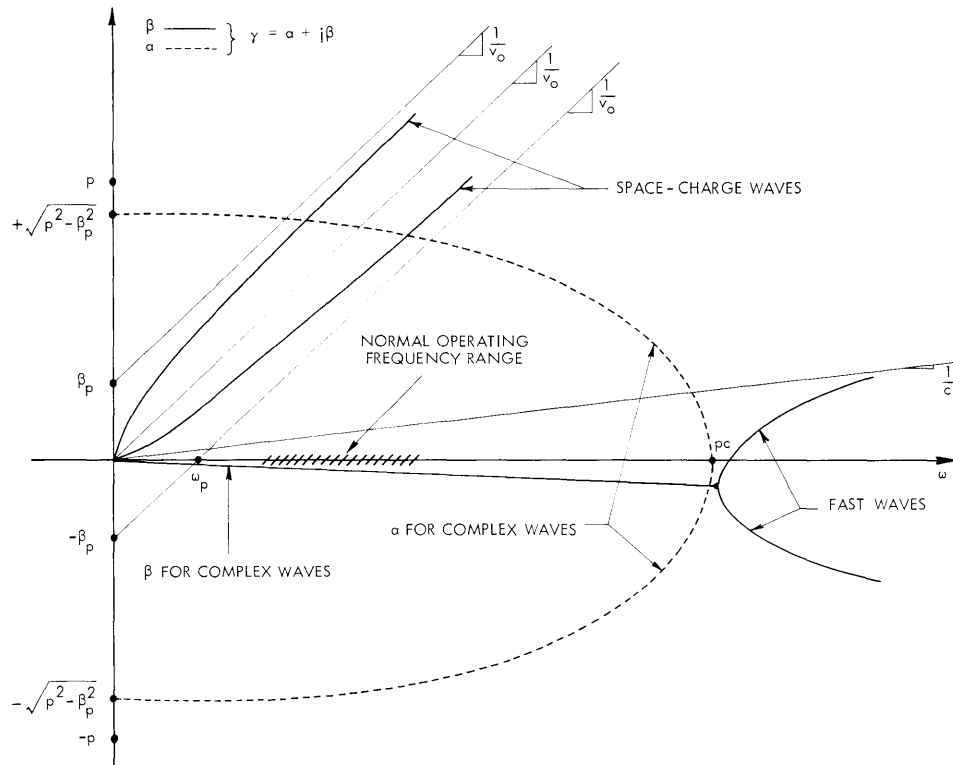
Fig. V-10. $\gamma(\omega)$ for $\beta_p < p$.
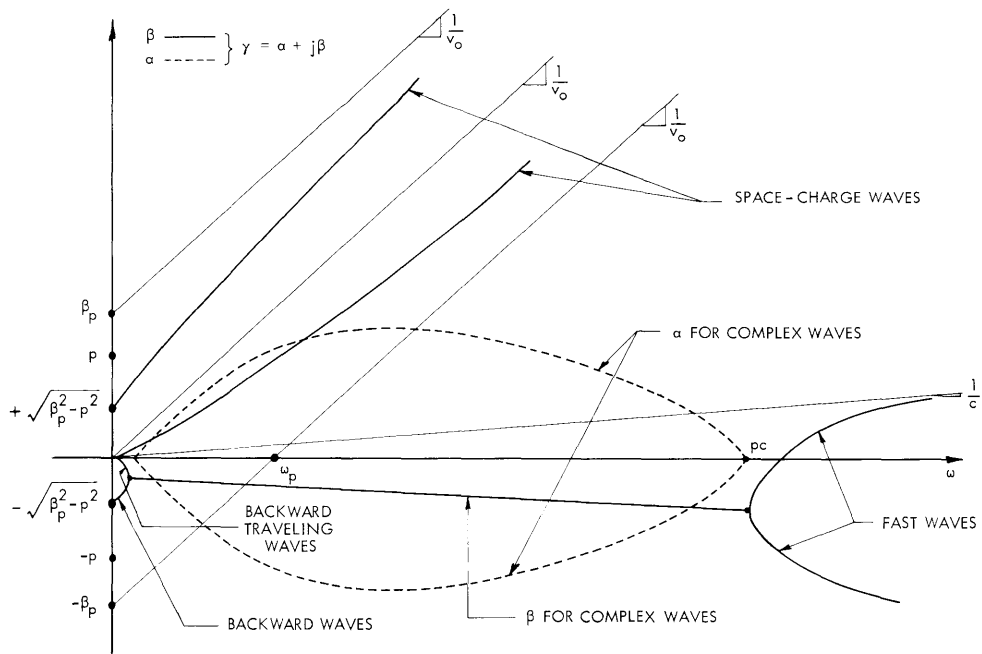

Fig. V-11. $\gamma(\omega)$ for $\beta_p > p$.

If $\beta_p > p$, the allowable roots γ will be as shown in Fig. V-11. At very low frequencies there are four pure imaginary solutions for γ: the space-charge waves plus the backward and backward-traveling waves.[5-7] There is still a frequency range for which there are two pure imaginary roots (space-charge waves) and two complex roots for γ. Finally, for frequencies above pc there are four imaginary roots: the two space-charge waves and the fast waves.

The latter case, $\beta_p > p$ (Fig. V-11), is not of any practical significance in microwave-beam devices, since present beam densities do not meet the condition $\beta_p > p$.

In practice, with $\beta_p < p$ (Fig. V-10), the frequency of operation of electron-beam devices is normally in the shaded region. In this frequency range there are two space-charge waves and two complex waves.

a. Complex Propagation Constant in a Hollow-Beam Waveguide

For most electron beams used in practice the complex propagation constants can be considered to arise from the perturbation by the electron beam of the empty-waveguide cutoff waves.

Perturbation theory for the propagation constant γ in a waveguide gives[8]

$$\gamma + \gamma_o^* = \frac{\int_A \tilde{J} \cdot \tilde{E}_o^* \, da}{\int_A (\tilde{E} \times \tilde{H}_o^* + \tilde{E}_o^* \times \tilde{H}) \cdot \bar{i}_z \, da}. \tag{3}$$

The subscript zero in Eq. 3 indicates an unperturbed quantity, while no subscript indicates a perturbed quantity. The tilde over a quantity signifies a complex vector that is only a function of the transverse coordinates; the integrations are over the cross-section area of the waveguide, and $\bar{i}_z$ is a unit vector in the z direction.
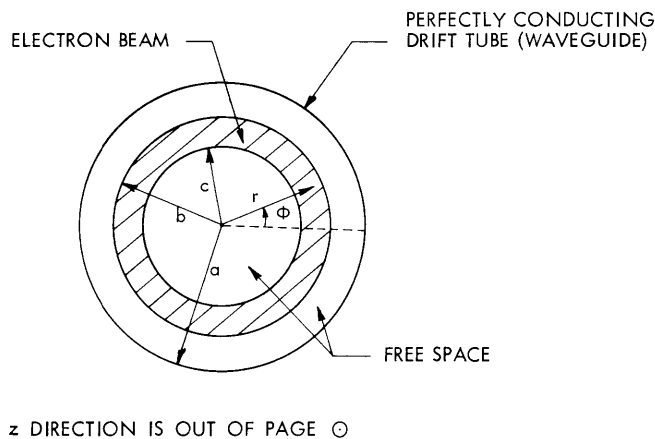

z DIRECTION IS OUT OF PAGE ⊙

Fig. V-12. Concentric-circular, hollow, electron-beam waveguide.

We shall assume that the unperturbed electric field $(\widetilde{E}_o)$ and magnetic field $(\widetilde{H}_o)$ belong to the empty-waveguide cutoff TM solutions with propagation constant $-a_o$. The perturbed electric field $(\widetilde{E})$ and magnetic field $(\widetilde{H})$ belong to the TM cutoff waveguide solutions with propagation constant a_o. The perturbed current density $(\widetilde{J})$ will be obtained from the electron-beam equations by using only the z-component of the perturbed empty-waveguide electric field for the longitudinal component of the electric field.

For a circular, hollow beam with the dimensions shown in Fig. V-12, the complex propagation constant $\gamma = a + j\beta$ in Eq. 3 becomes

$$a = a_o - \frac{p^2 \beta_p^2 \left(a_o^2 - \beta_e^2 \right)}{2a_o \left(a_o^2 + \beta_e^2 \right)^2} N \tag{4}$$

$$\beta = - \frac{p^2 \beta_p^2 \beta_e}{\left(a_o^2 + \beta_e^2 \right)^2} N, \tag{5}$$

where $p^2 = a_o^2 + k^2$ and

$$N = \frac{\int_c^b [J_o(pr)]^2 \, r dr}{\int_0^a [J_1(pr)]^2 \, r dr} \tag{6}$$

$$= \frac{b^2 \{[J_1(pb)]^2 + [J_o(pb)]^2\} - c^2 \{[J_1(pc)]^2 + [J_o(pc)]^2\}}{a^2 [J_1(pa)]^2} \tag{7}$$

2. Feedback in Klystrons Resulting from Complex Waves

Consider the configuration of two klystron-type cavities on an electron-beam wave-guide shown in Fig. V-13. The first cavity (upstream) is driven externally by a generator, while the output for the system is taken at the second cavity (downstream). As in all practical situations, we shall assume that the frequency of excitation at the upstream cavity lies in the shaded range of Fig. V-10.

Previous analyses included only the space-charge waves on the electron beam, with the result that the device was unilateral.[9] But the driven cavity will excite complex waves, as well as space-charge waves.[10] A complex wave with propagation constant γ ($\gamma = a+j\beta$, $a > 0$) will decay downstream from the first cavity; also, one with propagation constant $(-\gamma^*)$ decays upstream from this cavity. At the second cavity, a voltage
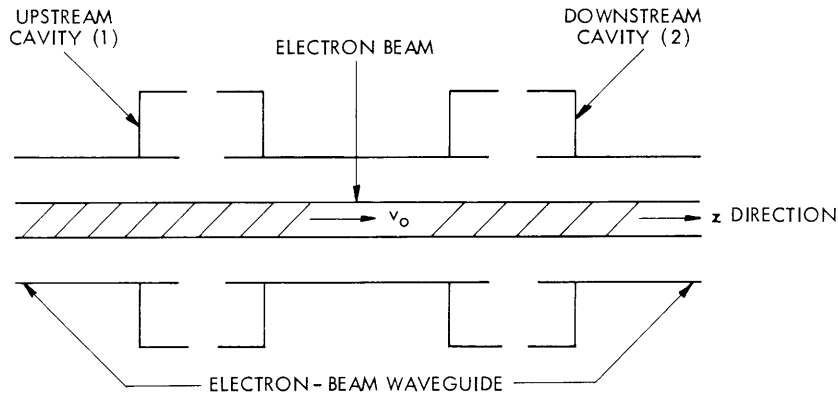
Fig. V-13.   Two cavities coupled to an electron-beam waveguide.

will be induced by the complex and space-charge waves that come from upstream.   At this cavity, in turn, space-charge waves continuing on downstream will be excited, but also, complex waves will be excited.   A complex wave with propagation constant $(-\gamma^*)$ will decay back upstream from the second cavity, and one with propagation constant γ decays on downstream.

Hence in the region between the two cavities there will be complex waves with propagation constants γ and $(-\gamma^*)$.   Such a pair of complex waves can carry the time-average power between the two cavities.   If these waves carry time-average power back upstream, the device will no longer be unilateral and the downstream cavity will affect the one upstream.   A scattering matrix formulation for these waves proves quite convenient.

a.   Scattering Matrix For a Single Gap[11]

The scattering matrix for the interaction of the fields in a single gap in the waveguide wall with the fields in the electron beam is defined by

$$
\begin{bmatrix} b_f \\ b_s \\ b_c \\ b_r \\ b_\ell \end{bmatrix} = \begin{bmatrix} s_{11} & s_{12} & s_{13} & s_{14} & s_{15} \\ s_{21} & s_{22} & s_{23} & s_{24} & s_{25} \\ s_{31} & s_{32} & s_{33} & s_{34} & s_{35} \\ s_{41} & s_{42} & s_{43} & s_{44} & s_{45} \\ s_{51} & s_{52} & s_{53} & s_{54} & s_{55} \end{bmatrix} \begin{bmatrix} a_f \\ a_s \\ a_c \\ a_r \\ a_\ell \end{bmatrix} \tag{8}
$$

or, in short notation,

$$\underline{b} = \underline{\underline{s}}\, \underline{a}. \tag{9}$$

Here, the double underscore indicates a matrix.   The wave amplitudes $\underline{b}$ and $\underline{a}$ are shown in Fig. V-14; the interaction region on the beam waveguide extends
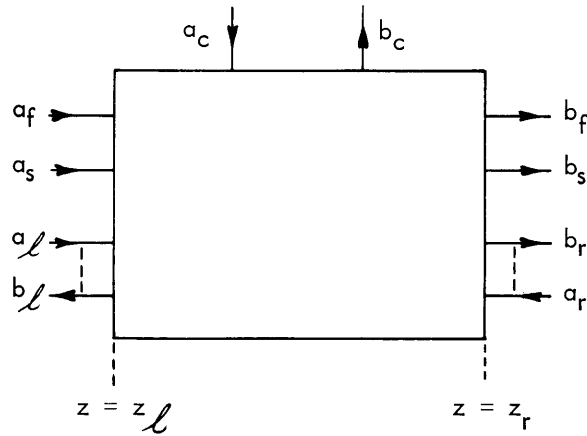
Fig. V-14. Wave amplitudes for the beam-gap interaction.

from $z = z_\ell$ to $z = z_r$.

The quantities a_c and b_c represent the amplitudes of the circuit waves; they are related to the conventional[9] gap voltage V_g and gap current I_g by

$$V_g = \sqrt{Z_0}\ (a_c + b_c) \tag{10}$$

$$I_g = \frac{1}{\sqrt{Z_0}}\ (a_c - b_c) \tag{11}$$

where Z_0 is an arbitrary normalization impedance. The quantities a_f and a_s are the amplitudes of the z-component of the electric field of fast and slow space-charge waves, respectively, normalized so that $\left(\frac{1}{2}\ |a_f|^2 - \frac{1}{2}\ |a_s|^2\right)$ represents the time-average power carried by these waves into the interaction region at $z = z_\ell$. Likewise, b_f and b_s are the amplitudes of the electric field of the fast and slow space-charge waves, respectively, normalized so that $\left(\frac{1}{2}\ |b_f|^2 - \frac{1}{2}\ |b_s|^2\right)$ is the real power carried out of the interaction

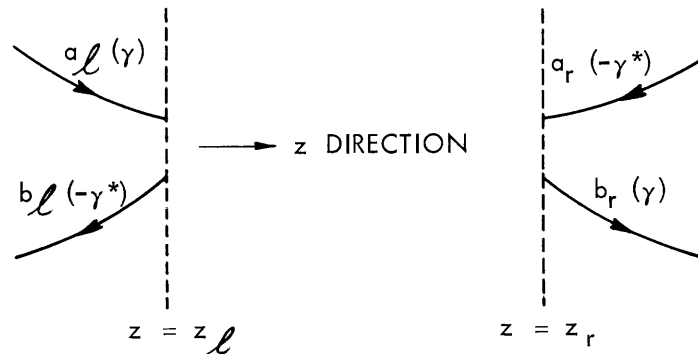

Fig. V-15. Complex wave amplitudes.

region at $z = z_r$ by the space-charge waves.

The z-component of the electric field at $z = z_\ell$ of the complex wave with propagation constant γ ($\gamma = \alpha + j\beta$; $\alpha > 0$) has amplitude a_ℓ, while that with propagation constant $(-\gamma^*)$ has amplitude b_ℓ. These amplitudes are normalized so that Im $(a_\ell b_\ell^*)$ represents the time-average power carried by the complex waves into the interaction region at $z = z_\ell$. Similarly, b_r is the amplitude of the complex wave with propagation constant γ at $z = z_r$, while a is associated with the complex wave $(-\gamma^*)$ at $z = z_r$. The time-average power carried out of the interaction region by the complex waves at $z = z_r$ is Im $(a_r^* b_r)$.

The scattering matrix element s_{33} may be found in terms of the electronic loading admittance $Y_{e\ell}^6$ by

$$\frac{1 - s_{33}}{1 + s_{33}} = Z_0 Y_{e\ell}.$$ (12)

The quantities s_{13} and s_{23} represent the excitation of the fast and slow space-charge waves, respectively, by the fields in the gap,[9-11] while the elements s_{43} and s_{53} are determined from the excitation of the complex waves by the fields in the gap.[10,11]

By applying conservation of energy flow and employing the drift-condition constraints,[9] it can be shown that all other elements of $\underline{s}$ in Eqs. 8 and 9 can be obtained from a knowledge of s_{13}, s_{23}, s_{33}, s_{43}, and s_{53}. The relations of all other elements to these known elements have been derived and are given elsewhere.[11]

b. Power Flow in Complex Waves

The two cavities shown in Fig. V-13 are represented formally in Figs. V-16 and V-17. The driven cavity has the scattering matrix $\underline{s}$, while the downstream cavity is represented by $\underline{S}$. We shall assume that there is no excitation on the beam entering the first cavity, so that $a_f = 0$ and $a_s = 0$. Also, there is no complex wave decaying into the upstream cavity region from the left, $a_\ell = 0$, and no complex wave decaying into the
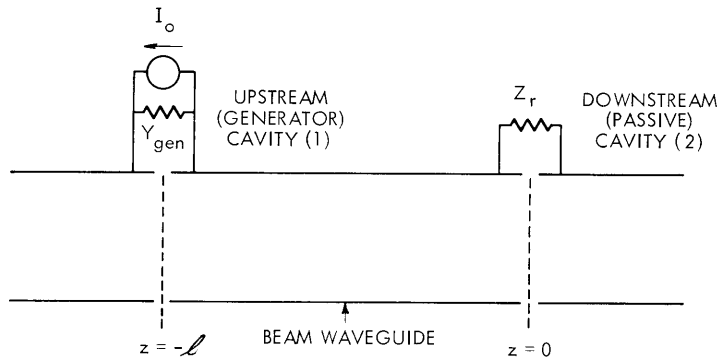

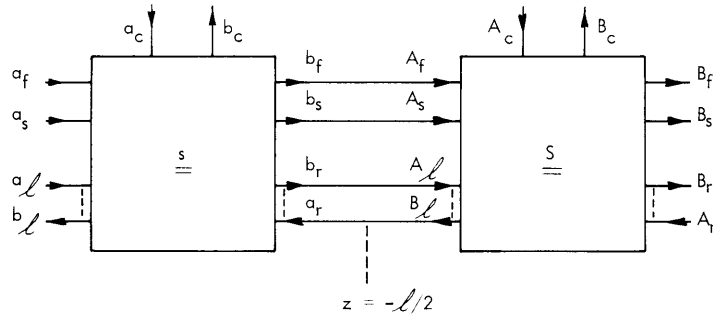Fig. V-16. Geometry for two cascaded cavities.

Fig. V-17.   Scattering matrices for two cascaded cavities.

downstream cavity region from the right, $A_r = 0$.

The external circuit at the driven cavity imposes the constraint

$$b_c = \Gamma_g a_c + c, \tag{13}$$

where

$$\Gamma_g = \frac{1 + Z_o Y_{gen}}{1 - Z_o Y_{gen}} \tag{14}$$

and

$$C = \frac{I_o \sqrt{Z_o}}{Z_o Y_{gen} - 1}. \tag{15}$$

The downstream cavity is passive, and hence

$$B_c = \Gamma_r A_c, \tag{16}$$

where

$$\Gamma_r = \frac{Z_r + Z_o}{Z_r - Z_o}. \tag{17}$$

The time-average power flow carried by the complex waves in the z direction (in the region between the two cavities) is

$$P_c = \text{Im}\left(a_r^* b_r\right) = \text{Im}\left(B_\ell^* A_\ell\right). \tag{18}$$

With the aid of Eqs. 13-18, P_c becomes

$$P_c = \left[\frac{|c|^2}{|s_{33}+f-\Gamma_g|^2}\right] \text{Im}\left[\frac{s_{43}}{s_{34}^*} f^* + \frac{s_{44}}{|s_{34}|^2}|f|^2\right], \tag{19}$$

where

$$f = \frac{s_{34}S_{53}[s_{13}S_{31}+s_{23}S_{32}+s_{43}S_{35}]}{Q^{-1}[s_{14}S_{31}+s_{24}S_{32}+s_{44}S_{35}]}$$

(20)

and

$$Q = \frac{(1+S_{33})(\Gamma_r - S_{33})}{\Gamma_r + 1}.$$

(21)

Note that if $Z_r = 0$, the second cavity is shorted. Then $P_c = 0$, since $\Gamma_r = -1$, $Q = \infty$, and $f = 0$. This is as expected, since no complex waves would be excited at the second cavity.

H. M. Schneider, A. Bers

References

1. W. C. Hahn, Small signal theory of velocity-modulated tubes, Gen. Elec. Rev. 42, 258 (1939).

2. S. Ramo, Space charge and field waves in an electron beam, Phys. Rev. 56, 276-283 (1939).

3. G. M. Branch and T. G. Mihran, Plasma frequency reduction factors in electron beams, IRE Trans., Vol. PGED-2, No. 2, pp. 3-11, March 1955.

4. R. J. Briggs and A. Bers, Fast waves in high-density electron-beam waveguides, Quarterly Progress Report No. 64, Research Laboratory of Electronics, M. I. T., January 15, 1962, pp. 48-51.

5. R. W. Gould and A. W. Trivelpiece, A new mode of wave propagation on electron beams, Proc. the Symposium on Electronic Waveguides, Vol. 8 (Polytechnic Press, Polytechnic Institute of Brooklyn, New York, 1958), pp. 215-228.

6. C. G. Alexander and A. Bers, Slow backward waves in an electron-beam waveguide, Quarterly Progress Report No. 59, Research Laboratory of Electronics, M. I. T., October 15, 1960, pp. 58-63.

7. A. Bers, Properties of waves in electron-beam waveguides, Quarterly Progress Report No. 61, Research Laboratory of Electronics, M. I. T., April 15, 1961, pp. 102-105.

8. H. A. Haus, Microwave Circuits, Notes for Course 6. 621, M. I. T., 1958.

9. A. Bers, Interaction of Electrons Wtih Electromagnetic Fields of Gaps With Application to Multicavity Klystrons, Sc. D Thesis, Department of Electrical Engineering, M. I. T., June 1959.

10. A. Bers, Electromagnetic waves in dense electron-beam waveguides and their interaction with electromagnetic fields of gaps, Quarterly Progress Report No. 58, Research Laboratory of Electronics, M. I. T., July 15, 1960, pp. 115-121.

11. H. M. Schneider, Complex Waves in Electron Beam Waveguides, S. M. Thesis, Department of Electrical Engineering, M. I. T., August 1963.